Journal of Contaminant Hydrology 123 (2011) 157–166

Contents lists available at ScienceDirect

Journal of Contaminant Hydrology

journal homepage: www.elsevier.com/locate/jconhyd

Evaluation of saline tracer performance during electrical conductivity groundwater monitoring

Micòl Mastrocicco [a], Henning Prommer [b,c], Luisa Pasti [d], Stefano Palpacelli [e], Nicolò Colombani [a,f,*]

[a] University of Ferrara, Department of Earth Sciences, Ferrara, Italy
[b] CSIRO Land and Water, Wembley, Western Australia, Australia
[c] School of Earth and Environment, University of Western Australia, Crawley WA 6009, Western Australia
[d] University of Ferrara, Department of Chemistry, Ferrara, Italy
[e] Politechnical University of Marche, Engineering Department, Ancona, Italy
[f] University of Rome "La Sapienza", Department of Earth Sciences, Roma, Italy

ARTICLE INFO

Article history:
Received 13 June 2010
Received in revised form 22 October 2010
Accepted 13 January 2011
Available online 22 January 2011

Keywords:
Saline tracers
Electrical conductivity
Aquifer parameters
Cation exchange
Modelling

ABSTRACT

Saline solutions are the most commonly used hydrological tracers, because they can be easily and economically monitored by in situ instrumentation such as electrical conductivity (EC) loggers in wells or by geoelectrical measurements. Unfortunately, these low-cost techniques only provide information on the total concentration of ions in solution, i.e., they cannot resolve the ionic composition of the aqueous solution. This limitation can introduce a bias in the estimation of aquifer parameters where sorption phenomena between saline tracers and sediments become relevant. In general, only selected anions such as Cl^- and Br^- are recognised to be transported unretarded and they are referred to as conservative tracers or mobile anions. However, cations within the saline tracer may interact with the soil matrix through a range of processes such as ion exchange, surface complexation and via physical mass-transfer phenomena. Heterogeneous reactions with minerals or mineral surfaces may not be negligible where aquifers are composed of fine alluvial sediments. The focus of the present study was to examine and to quantify the bias between the aquifer parameters estimated during model-based interpretation of experimental data of EC measurements of saline tracer relative to the aquifer parameters found by specific measurements (i.e. via ionic chromatography, IC) of truly conservative species. To accomplish this, column displacement experiments with alluvial aquifer materials collected from the Po lowlands (Italy) were performed under water saturated conditions. The behaviour of six selected, commonly used saline tracers (i.e., LiCl, KCl, and NaCl; LiBr, KBr, and NaBr) was studied and the data analysed by inverse modelling. The results demonstrate that the use of EC as a tracer can lead to an erroneous parameterisation of the investigated porous media, if the reactions between solute and matrix are neglected. In general, errors were significant except for KCl and KBr, which is due to the weak interaction between dissolved K^+ and the sediment material. The study shows that laboratory scale pre-investigations can help with tracer selection and to optimise the concentration range targeted for in situ multilevel monitoring by unspecific geoelectrical instrumentation.

1. Introduction

In the Po plain (Italy), like in many other parts in the world, unconfined shallow aquifers are often severely polluted. The area not only suffers from point source pollution such as leaking oil tanks, pipelines, chemical facilities and landfills (Burbery et al., 2004; Colombani et al., 2009; Giuliano, 1995) but also from a

* Corresponding author. University of Ferrara, Department of Earth Sciences, Ferrara, Italy.
E-mail address: clo@unife.it (N. Colombani).

0169-7722/$ – see front matter © 2011 Elsevier B.V. All rights reserved.
doi:10.1016/j.jconhyd.2011.01.001

range of diffuse pollution sources resulting from the excessive application of agrochemicals (Accinelli et al., 2002; Barra Caracciolo et al., 2005; Onorati et al., 2006). In such aquifers tracer tests are a crucial and regularly employed method to characterise some of the key hydrogeological parameters that control contaminant fate and transport (Benker et al., 1997; Ptak et al., 2004; Thierrin et al., 1995). Unfortunately, comprehensive tracer tests require a substantial effort in terms of chemical analysis of a large number of samples, especially where grids of multilevel sampling wells are involved (Rajaram and Gelhar, 1991; Sudicky, 1986). Numerous techniques have been developed to limit the duration of experiments and therefore to minimise sampling and analytical costs. Forced gradient tracer tests, for example, allow for faster breakthrough times by increasing natural groundwater velocities (Chen et al., 1999; Sutton et al., 2000). However, sampling requirements in many cases might not be dictated by the absolute length of the experimental period, but rather by the temporal resolution required to resolve breakthrough signals at sufficient detail. Therefore the high cost for sampling and chemical analysis may be more efficiently reduced by employing in situ instruments that provide continuous measurements. Most notably, electrical conductivity probes equipped with data loggers have been commonly employed to identify the parameters governing nonreactive solute transport both in the laboratory (Choi et al., 2007; Guber et al., 2005) and in the field (Cirpka et al., 2007; Vogt et al., 2010). Also, a range of geophysical techniques like time domain reflectometry (Comegna et al., 1999; Munoz-Carpena et al., 2005), electrical resistivity tomography and induced polarization (Cassiani et al., 2006; Hördt et al., 2007; Slater, 2007) have been successfully applied to determine solute transport parameters. All of these techniques can only be used with confidence as long as a robust relationship between the monitored electrical property and the tracer concentration holds true under the site-specific conditions (Rhoades et al., 1989). For instance, a linear relation between the EC of a solution and concentration of a saline tracer is generally applicable and valid for all cases where the soil matrix has little ion sorption capacity. However, even under these conditions there are several factors that can influence the usefulness of EC measurements at field sites, such as temperature, water content, ionic composition (Rein et al., 2004) and organic pollutants (Atekwana et al., 2004). Also, natural, temporal variability in the ambient water composition can mask the electrical conductivity signal that originates from a salt tracer injection.

The aim of the present work is to highlight the potential errors and limitations of low-cost electrical conductivity loggers in obtaining reliable data for the characterisation of alluvial aquifers via saline tracer tests and to understand the physico-chemical processes controlling the transport behaviour of the various tracers. A series of column experiments using sediments typical and representative of the Po plain lowlands was carried out. The miscible displacement tests were set up to compare the most widely used saline tracers, including LiCl, KCl, NaCl, LiBr, KBr and NaBr (Davis et al., 1985; Käss, 1998), at different flow rates and concentrations. Effluents were monitored with EC loggers and analysed for all major cations and anions by ion chromatography. The tracer results were analysed by inverse tracer transport and reactive transport modelling, using both the classical advection dispersion equation (ADE) and the dual domain (DD) formulation.

2. Materials and methods

2.1. Sediments collection and characterisation

Sediment material was collected at the L.A.R.A. ENVIREN Hydrogeology Field Site situated inside the F.lli Navarra Foundation for Agriculture, near Ferrara (NE Italy). The material was sourced from the unconfined section of the aquifer, which consists of recent fluvial sandy deposits from 0.8–1 m to 5–6 m below ground surface (bgs). An auger equipped with a sediment sampler at a depth between 1.5 and 2.5 m bgs was used for collection. Two series of 5 sediment samples of alluvial materials from two different depth intervals of 1.5–2 and 2–2.5 m bgs (0 to 1.5 m below the water table) were collected. The five samples from each depth interval were mixed and a physical characterisation was performed for both of the two resulting mixtures in triplicates, referred to as Column 1 and Column 2 (See Table 1 for results).

Particle size curves were obtained using a sedimentation balance for the coarse fraction and an X-ray diffraction Sedigraph 5100 Micromeritics for the finer fraction; the two regions of the particle size curve were connected using the computer code SEDIMCOL (Brambati et al., 1973). Constant pressure head tests were used to infer the average hydraulic conductivity of each column, while bulk density and water content were determined gravimetrically. The gravimetric water content was measured for saturated condition (after elution of a volume corresponding to 100 pore volumes). The residual water content was measured gravimetrically in triplicates on air dried sediments after being heated for 24 h at 105 °C.

The Cation Exchange Capacity (CEC) was estimated using a three step displacement method (Sullivan et al., 2003), for both sediments in triplicates (Table 1). In the first step ½ g of sediment was shaken for at least 1 h with 30 ml of 1 M of NaCl solution. The mixture was then centrifuged and the supernatant was decanted off in a container. This procedure was repeated two more times, with the supernatant from each step being combined with that from the previous steps, creating a final solution of 90 ml analysed for major cations via ion chromatography.

2.2. Chemical analysis

Two LTC M10 Levelogger Solinst® data loggers were placed in a flow-through chamber at the column inlet and outlet to continuously monitor electrical conductivity and

Table 1
Sediment characteristics and their mean ± of the standard deviation.

Parameter	Column 1	Column 2
Grain size (%)		
Coarse sand (630–2000 μm)	0.00 ± 0.00	1.00 ± 0.01
Medium sand (200–630 μm)	7.6 ± 0.12	5.1 ± 0.004
Fine sand (63–200 μm)	66.3 ± 0.3	52.8 ± 0.4
Silt (2–63 μm)	21.3 ± 0.1	32.2 ± 0.2
Clay (<2 μm)	4.8 ± 0.04	9.0 ± 0.05
Hydraulic conductivity (m/s)	$1.7e^{-5} \pm 2e^{-6}$	$4.8e^{-6} \pm 2e^{-6}$
Bulk density (Kg/m^3)	1.63 ± 0.01	1.57 ± 0.01
Gravimetrical water content (%)	35.5 ± 0.01	36.8 ± 0.01
Residual water content (%)	3.7 ± 0.02	4.8 ± 0.03
Total porosity (%)	39.2 ± 0.03	41.6 ± 0.04
CEC (meq/L)	5.57 ± 0.4	10.6 ± 2.1

temperature. The four electrode platinum conductivity sensor was calibrated using four standard calibration points. An automatic temperature compensation provided an EC accuracy of ± 10 μS/cm. The double data logger system employed for the experiments permitted identification and elimination of occasional EC oscillations within the influent water, and thus maintenance of a stable base line. A fraction collector Pharmalab TSC110 was employed to collect 5 ml effluent fractions downstream from the inline EC logger. The measured EC values were converted to dissolved saline tracer concentrations using a linear relationship that was determined from five calibration points. The calibration procedure indicated a reliable linear correlation for all tracers used in this study. Aqueous samples from the column effluent end were obtained with an AS-40 Dionex auto-sampler and the major cation and anion concentrations were determined by analysis with an isocratic dual pump ion chromatography (IC) ICS-1000 Dionex. Three replicates were performed for each sample to determine the standard deviations. The analytical accuracy was found to be better than 2% for anions and better than 5% for cations.

2.3. Column transport experiments

Column experiments were conducted using Perspex columns with an inner diameter of 10 cm and a height of 100 cm, as described earlier in Mastrocicco et al. (2009). Columns were packed with air dried bulk sediments as collected at the field site and the packing was performed with incremental layers of 3 ± 0.5 cm excluding aggregates with dimensions larger than 2 ± 0.1 cm. Prior to the experiments, sediments were flushed with tap water for more than 100 pore volumes to achieve complete chemical equilibrium between water and sediments. Once a stable flow rate of 5 ml/min (~2.3 m/d) was established, breakthrough experiments were performed in both columns by injecting, for every saline tracer, 100 ml of solution. A double port switch injector created a pulse input of 2.0 g/l for every saline tracer. As soon as the injection of the tracer solution was completed, inflow was switched back to tap water while maintaining steady-state flow conditions. Flushing then continued for at least another 100 pore volumes. The sum of the gravimetric and the residual water content is referred to as the total porosity θ. Pore volumes of water in the column, Pv (cm^3/cm^{-3}) were defined as:

$$P_v = \theta \pi r^2 L \tag{1}$$

where r is the inner radius of the soil columns (cm) and L is the length of the soil column (cm), and were calculated to be 3079 cm^3 and 3267 cm^3 for Columns 1 and 2, respectively. To determine changed responses due to the flow rate and tracer concentrations, additional breakthrough experiments were carried out with input tracer concentrations of 0.5 and 1.0 g/l, and flow rates of 10 and 1 ml/min, respectively.

The experiments resulted in a tracer breakthrough. This breakthrough is given as BTCs. The experimental BTCs were corrected by subtracting the measured extra-column volume of the tubing (25 ml) and of the flow-through chamber (80 ml). Both the IC-derived BTCs of Br^- and Cl^- and the EC-derived saline tracer BTCs were analysed with the temporal moment method (Eriksson et al., 1997). Thereby the normalized zeroth moment, M, quantifies the fraction of tracer mass recovered in the effluent. The computation of the normalized first moment, μ_1, which corresponds to the mean arrival time of the tracer, was computed to define the linear retardation factor R. The normalised central second moment, μ_2, provided a measure of the spreading of the tracer relative to the centre of mass. Finally, the skewness S of the BTC was computed from the ratio $\mu_3/(\mu_2)^{1.5}$, whereby μ_3 is the normalized third central moment (Vincent et al., 2007).

2.4. Modelling approach

2.4.1. Inverse modelling

The measured BTCs were further analysed with CXTFIT 2.1 (Toride et al., 1999), which can solve the ADE in parameter estimation mode to fit the observed concentrations. In addition to the standard ADE, CXTFIT also implements a DD formulation that accounts for physical non-equilibrium processes. In this formulation, the pore space is conceptually divided into two distinct domains, mobile and immobile domains. In the mobile domain, transport is assumed to be governed by advection and hydrodynamic dispersion. Within the immobile domain, no advective transport is assumed to occur. Mass exchange between both domains is assumed to occur through a rate-limited mass-transfer process. In the model, the total porosity (θ) is separated into a fraction representing the mobile domain (θ_m) and a fraction representing the immobile domain (θ_{im}). The mass conservation equation for the DD approach is (Van Genuchten and Wierenga, 1976):

$$\theta_m \frac{\partial C_m}{\partial t} + \theta_{im} \frac{\partial C_{im}}{\partial t} = \theta_m D_m \frac{\partial^2 C_m}{\partial x^2} - \theta_m v_m \frac{\partial C_m}{\partial x} \tag{2}$$

where C_m (ML^{-3}) and C_{im} (ML^{-3}) denote the mobile and immobile solute concentrations as functions of distance x (L) and time t (T). Under steady-state flow conditions, the hydrodynamic dispersion coefficient for the mobile region D_m (L^2T^{-1}), the mean mobile pore–water velocity v_m (LT^{-1}), and the volumes θ (L^3L^{-3}), θ_m, (L^3L^{-3}), and θ_{im} (L^3L^{-3}) are assumed to be constant. D_m is defined as $D_m = \lambda_L v_m$, where λ_L (L) is the longitudinal dispersivity. When $\theta_m = \theta$, Eq. (2) reduces to the single-domain ADE. The solute–mass transfer between mobile and immobile regions is defined as:

$$\theta_{im} \frac{\partial C_{im}}{\partial t} = \alpha (C_m - C_{im}) \tag{3}$$

where α ($L^3L^{-3}T^{-1}$) is a rate coefficient. Eq. (4) is combined with Eq. (1) to give:

$$\theta_m \frac{\partial C_m}{\partial t} = \theta_m D_m \frac{\partial^2 C_m}{\partial x^2} - v_m \theta_m \frac{\partial C_m}{\partial x} - \alpha (C_m - C_{im}) \tag{4}$$

The main characteristics that distinguish the DD from the ADE BTCs of a tracer are the so called "early breakthrough", related to accelerated transport via preferential pathways and "tailing", due to diffusion driven processes into stagnant zones. Thus, with increasing importance of preferential pathways and stagnant zones the ADE becomes increasingly inappropriate while solute transport behaviour can still be

successfully described by the DD approach. In the numerical models the 1 m long experimental columns were discretized into 100 grid cells. The hydraulic conductivities and porosities attributed to these grid cells are listed in Table 1. A constant head boundary was used at both the influent and effluent ends of the column to simulate steady-state flow rates. The tracer pulse was simulated as a time pulse input boundary condition. CXTFIT was run in inverse mode to estimate (i) λ_L where the BTCs were simulated via single-domain ADE and (ii) λ_L, θ_{im}, and α where the DD approach was employed.

2.4.2. Reactive transport modelling

Additional reactive transport simulations were performed for a selected experiment to identify and quantify in detail the solute–sediment interactions, in conjunction with physical non-equilibrium processes. The simulations elucidated the heterovalent multi-component cation exchange reactions, which allow the selective displacement/replacement of cations that occurs on clay minerals, organic matter and hydroxides (Appelo and Postma, 2005). The reactive multi-component transport code, PHT3D (Prommer et al., 2003; Greskowiak et al., 2010), which can simultaneously account for complex geochemical reactions and dual domain behaviour was used for this purpose. The local equilibrium assumption (LEA) was assumed to hold for the simulated chemical reactions, i.e., the competition of four exchangeable cations (Ca^{2+}, Na^{+}, Mg^{2+}, and K^{+}) for one type of exchanger site. This was also suggested by our calculated Damköhler numbers (e.g., Valocchi, 1985) which were always >100 for all the investigated flow rates. The reactive model was implemented to simulate a 20 min long injection of a 1 g/l tracer solution (NaCl) into Column 2, followed by a flushing period of 1.1 days. The column was discretized by a one dimensional model of 100 grid cells, each of 1 cm length. The initial and inflow water compositions used in the model are listed in Table 2.

3. Results and discussion

3.1. Experimental results

3.1.1. Mass recovery

Measured solute elution curves were analysed by plotting the normalized measured leachate concentration (i.e., the ratio of the measured effluent concentration and the injected pulse concentration, C_0) versus the number of pore volumes eluted, defined as V/V_0, where V is the flux-averaged volume of solute eluted (cm^3) and V_0 is the volume of water in the column (cm^3).

Fig. 1 shows concentrations of Cl^- (Fig. 1a and c) and Br^- (Fig. 1b and d), as measured by IC for the fractions collected from the column output, and, in comparison, the EC-derived curves as measured directly on the eluate. It can be seen that the shape of the BTCs determined by EC and IC differ, particularly with respect to the peak shape. The EC-derived curves exhibit a clearly longer tailing than those determined by IC, specifically the BTCs for Column 2. In order to quantify the difference between the elution profiles, a temporal moment analysis was performed (Table 3). The results indicate that the mass recovery estimates from the calculation of the zeroth moment for the EC-derived data from the experiments where KCl or KBr were utilised as saline tracers are essentially similar to those determined for the conservative ions Br^- and Cl^- (analysed by IC). However, in all the other cases the EC-derived data lead to an overestimation of the injected mass. The deviation in the computed mass is in the worst case (i.e., for LiCl) +25% for Column 1 and +67% for Column 2.

3.1.2. Retardation

R values estimated from the EC logged data are generally greater than those estimated from the conservative, IC-determined anion tracers Cl^- and Br^-. This originates mainly from the tailing of the EC peaks, which causes the centre of mass to be shifted. For Column 1, the bias in *R* estimation from EC-derived data decreases in the order LiBr>LiCl>NaBr>NaCl>KBr>KCl. A more complex breakthrough behaviour was observed for Column 2. Here the order of the computed retardation factors is NaBr>LiBr>NaCl>LiCl>KBr>KCl. By comparing the *R*(EC) values of the saline solutions with those of the correspondent anion (i.e., Br^- and Cl^-) the bias increases as: $Na^+>Li^+>K^+$. In the literature it is generally recognised that the relative affinity of ion exchange surfaces of alkali metal is: $K^+>Na^+>Li^+$ (Lyman et al., 1990). However, both the ionic strength of the medium and the salt concentration have an influence in the exchange equilibriums. Considering that ionic mobility in water decreases with the order $K^+>Na^+>Li^+$, the observed *R*(EC) values follow the same trend. This observation suggests that the elution is governed by percolation.

Moreover, a more complex behaviour was observed in Column 2. In this case the *R*(EC) values followed the subsequent order: NaBr>LiBr>NaCl>LiBr>KBr>KCl. Comparing the *R*(EC) values of saline solutions to those of the correspondent anion (i.e. Br^- and Cl^-) it can be seen that the bias increases as: $Na^+>Li^+>K^+$.

Differences in the behaviour of saline tracers recorded by EC loggers in the two columns were due to specific interaction between solutes and sediments. In particular, since the ionic nature of the solute and the fact that observed differences are mainly due to the cation type, it seems that these differences arise from cation exchange interactions.

3.1.3. Dispersion and skewness

To further investigate the behaviour of the saline tracers, the mass spreading around the centre of mass (peak dispersion) was evaluated by determining the second central moment of the BTCs. From Table 3 it can be seen that the dispersion

Table 2
Initial and inflow water composition used in the PHT3D simulations of the NaCl tracer experiment in Column 2.

Aqueous components	Initial water composition and flushing solution [mg/L]	Tracer solution [mg/L]
Ca	35.0	37.8
Mg	12.0	12.9
Na	12.1	401.4
K	2.8	2.1
Cl	24.9	597.6
N(5)	5.5	5.6
S(6)	37.0	39.9
pH	7.6	7.5
pe	4.5	4.2

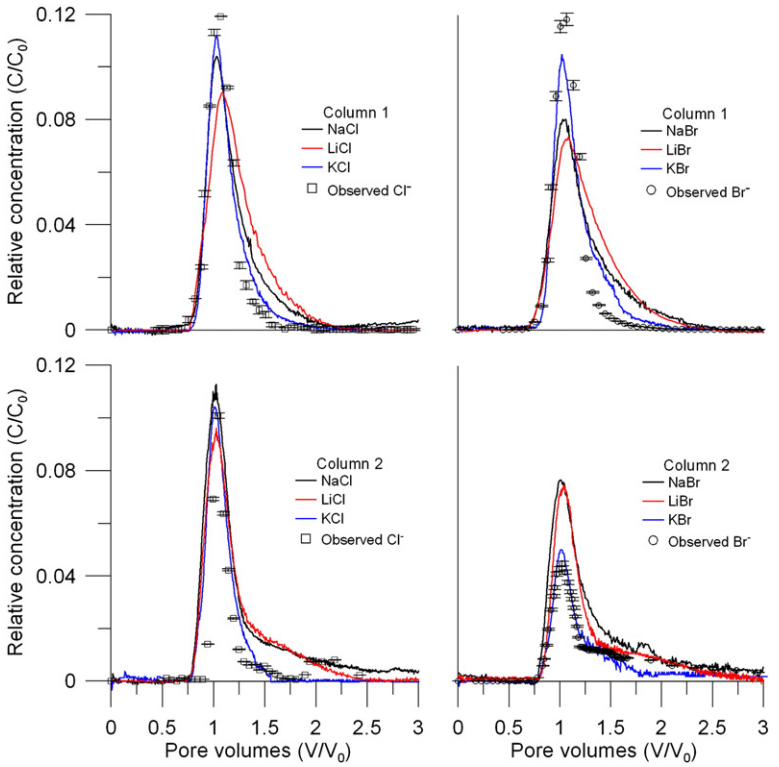

Fig. 1. Measured Cl^- (left) and Br^- (right) breakthrough data in comparison with continuously logged EC data for various saline tracers with input concentration of 2 g/l (C_0). The upper panel shows results for Column 1 and the lower panels show results for Column 2. Error bars are plotted for Cl^- and Br^-.

calculated from the EC-derived BTCs of the saline tracers (μ_2 in Table 3) is larger than that of the IC-determined Br^- and Cl^- BTCs, except for KCl and KBr. Both, KCl and KBr show μ_2 values that are similar to those recorded for Br^- and Cl^-.

Finally the skewness of the BTC data was analysed. A positive skewness indicates a longer tail after peak breakthrough, from the comparison between the skewness values of the saline solutions and the correspondent anion chemical reactions can be estimated. A perfectly symmetric shape of the BTC results in a skew equal to 0 (King and Julstrom, 1982). From the computed values listed in Table 3 it is clear that both Br^- and Cl^- as well as all the EC-derived saline tracer BTCs show a tailing effect, although of variable extent. Thus, it is not possible from the moment analysis alone to clearly differentiate physical non-equilibrium processes from chemical reactions.

Table 3
Temporal moment analysis of BTCs in Column 1 and 2, *M* is the mass recovery, *R* is the retardation factor, μ_2 is the spreading around the centre of mass and *S* is the skewness.

	Column 1				Column 2			
Tracer	*M*	*R*	μ_2	*S*	*M*	*R*	μ_2	*S*
Br^-	99.7	1.03	0.04	1.15	93.8	1.00	0.08	1.27
Cl^-	95.4	1.02	0.03	1.19	99.9	1.01	0.07	1.25
EC-NaCl	120.5	1.13	0.08	1.44	167.1	1.12	0.42	2.82
EC-NaBr	112.2	1.14	0.14	1.28	142.9	1.18	0.35	2.11
EC-LiCl	125.3	1.16	0.07	0.87	144.3	1.11	0.24	1.55
EC-LiBr	113.1	1.19	0.09	0.79	122.6	1.14	0.23	1.99
EC-KCl	100.4	1.08	0.05	1.17	101.3	1.04	0.09	1.08
EC-KBr	101.8	1.10	0.07	1.09	99.9	1.06	0.09	1.09

3.1.4. Impact of flow rates and salt concentrations

To identify the processes that cause this observed tailing, a series of additional experiments was conducted, where flow rates and salt concentrations were varied systematically. In these experiments LiCl served as the saline tracer. EC data was again logged continuously. Fig. 2 shows the results of these experiments. It can be noticed that the tailing of the LiCl BTCs increases with increasing flow velocity; this behaviour is similar for all the examined salt concentrations, as shown by the calculated *S* values in Table 4.

When the sample mass injected begins to exceed the capacity of a specific site type that interact with the cations, the peak tailing increases, the front of the peak will become sharper and the back of the peak will tail more. Another clue that the column is being overloaded is that retention will decrease as greater sample mass is injected (Giddings, 1965). Moreover, from column experiments it can be seen that flow rate and salt concentration are important factors in determining peak parameters which, in turn, can be employed to infer hydrological parameters.

These results indicate that the moment analysis of EC-derived data alone is insufficient to generate a unique set of aquifer parameters. Inverse modelling employing different conceptual models was therefore used to further analyse the measured BTCs obtained from IC-determined Br^- and EC-derived LiCl data, respectively.

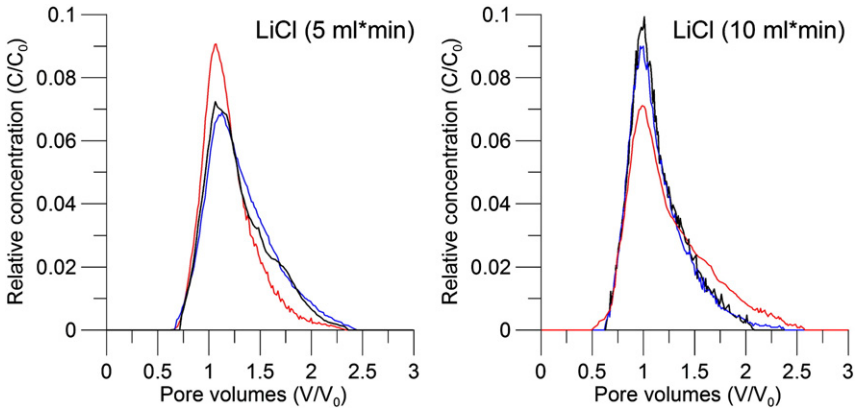

Fig. 2. Comparison of LiCl breakthrough curves with EC logging for different concentrations of 2000 mg/L in red, 1000 mg/L in blue and 500 mg/L in black and flow rates (black lines are 5 mL/min and blue lines are 10 mL/min) in Column 1.

3.2. Inverse modelling

The results of the inverse model simulations display, in many cases, a good fit with the measured Br^- concentration data (Fig. 3). Particularly the use of the DD approach resulted in favourable model fits. This is indicated by average regression coefficients (R^2) of 99.6% and 98.2%, for Columns 1 and 2 respectively (Table 5). On the other hand, using the ADE approach for the simulation of Br^- BTCs resulted generally in less favourable model fits, as indicated by the lower R^2 values of 92.0% for Column 1 and 85.2% for Column 2, respectively. The EC-derived LiCl BTCs were not well reproduced by the ADE approach, as illustrated in Fig. 3.

The ADE approach, in particular, failed to reproduce the observed tailing, which was most obvious in the case of Column 2, where the tailing is more pronounced. Consequently, larger λ_L values were determined by inverse modelling (Table 5), i.e., values that were >100% above those obtained from the corresponding DD models.

The DD approach provided a better fit of the EC-derived LiCl BTCs for both columns. Nevertheless, since the observed tailing needs at least partially to be attributed to ion exchange reactions between the cations contained in the saline tracer and the sediment material (as discussed earlier), the good model fit may not directly imply a correct conceptual model and parameterisation of the aquifer material. This problem is indicated by the different parameter values that were inferred from the EC-derived BTCs and from the IC BTCs. The comparison of results shows that the DD parameters obtained from the LiCl BTCs for Column 2 were different from the DD parameters (Table 5) obtained from the Br^- BTCs. On the other hand, for Column 1, where CEC was lower, all the LiCl BTC fitted DD parameters were essentially similar to those for the DD parameters obtained from Br^- BTCs, except for λ_L. The discrepancy between parameter values gained from the EC-derived LiCl BTCs and those gained from the IC data implies that the physical mass-transfer process alone, as simulated by the DD approach is not sufficient to accurately represent the mechanisms that control the shape of the BTCs. Therefore, in the following we investigate which role geochemical reactions might have played on the modification of the observed BTCs. The 1 g/l NaCl injection experiment in Column 2 was selected for this analysis, as it exhibited a particularly large tailing effect.

Table 4
Temporal moment analysis of EC-derived LiCl BTCs in Column 1 at different flow rates and influent concentrations.

	Q (5 ml*min)				Q (10 ml*min)			
EC-LiCl	*M*	*R*	μ_2	*S*	*M*	*R*	μ_2	*S*
2000 mg/l	120.8	1.12	0.08	0.07	116.1	1.13	0.09	0.97
1000 mg/l	110.0	1.06	0.14	0.08	104.2	1.21	0.06	0.61
500 mg/l	113.3	1.05	0.07	0.08	110.7	1.19	0.07	0.65

3.3. Reactive transport modelling

In the reactive transport model the solute–sediment interaction was explicitly considered through an equilibrium cation exchange model instead of the linear equilibrium sorption model that was employed in the inverse modelling with CXTFIT. The model parameters that were adjusted during calibration were: the Cation Exchange Capacity (CEC), the mass-transfer rate coefficient (α) and both the volume fraction occupied by the mobile (θ_m) and the immobile domain (θ_{im}). In contrast to the CXFIT model calibration, the calibration of the reactive transport model considered observed BTCs from multiple ions (Na, Ca and Cl) as calibration constraints.

Fig. 4 shows manually calibrated simulation results for Cl^- and two reactive components, Na^+ and Ca^{2+} in comparison with measured concentration. The figure also shows the comparison with results from simulations where selected individual processes were neglected. This comparison illustrates that the full reactive model, which includes exchange reactions in combination with DD, provides the best agreement with the observed results, while the alternative simpler approaches failed to fit the observed data. In the observed Na^+ and Ca^{2+} BTCs a double peak is noticeable, which was most likely resulting from changes in the influent tap water composition. Obviously, both ADE and DD fail to reproduce the retardation of the BTCs of Na^+ and Ca^{2+} in the absence of the exchange reactions. In addition the application of the ADE in combination with exchange reactions over predicts concentrations of both cations and anions. Note that the calibrated CECs were approximately 4 times below the analytically determined values. This discrepancy can partially be attributed to the

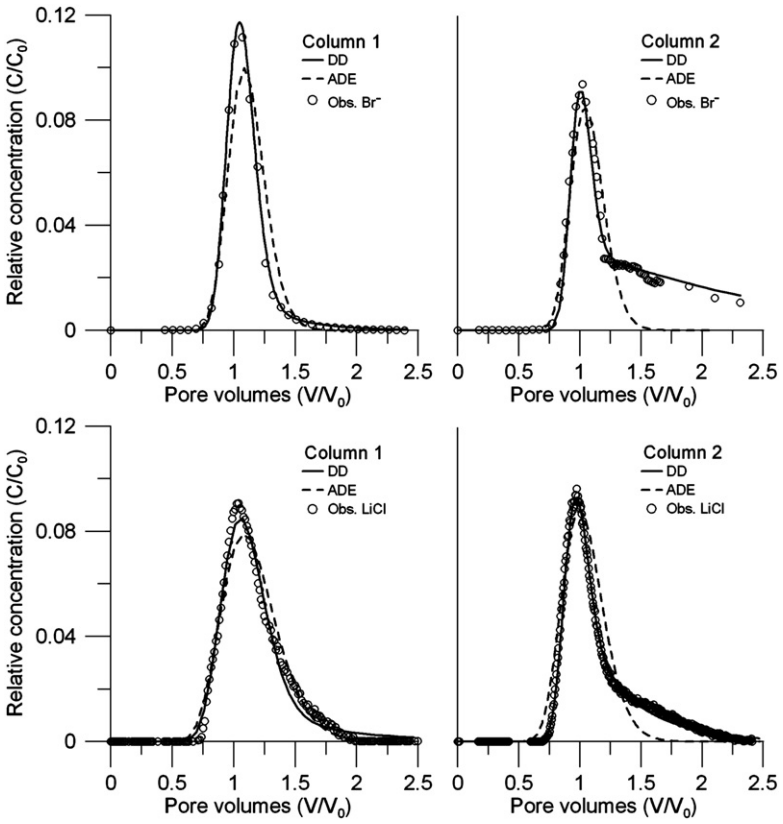

Fig. 3. Comparison of Br^- and LiCl BTCs versus model results using two alternative approaches, ADE and DD, for Column 1 and Column 2.

variability of the analytical results, as expressed by the mean of the standard deviation in Table 1. However, a systematic bias may also be attributed to the fact that access by physical mass-transfer processes to some of the existing exchanger sites in the immobile domain was (much) slower than that considered by the single rate mass-transfer model employed in these simulations.

3.4. Evaluation of the bias in transport parameters estimation

The estimation of λ_L via inverse modelling resulted in significant deviations between the values obtained from Br^- and the values obtained from the analysis of the LiCl BTCs, especially when the underlying model for the interpretation assumed that the ADE was valid (Table 5). Excessively large λ_L values were obtained for both columns when attempting to match the broad peaks produced by the LiCl tracer solution. Overall the ADE approach failed to reproduce the details of the observed BTCs for both Br^- and LiCl tracers. This failure is because for both columns a portion of the total porosity was identified as being in an immobile zone (see Table 1). The DD model approach, which conceptually incorporates the effects induced by immobile zones, was therefore able to produce a much better fit with the observed concentrations. However, different parameter values were still obtained for Br^- and LiCl in both columns (Table 5). The more comprehensive reactive transport simulations of the NaCl tracer experiment in Column 2 were able to reconcile these discrepancies by considering an improved description of the ion exchange process. Fig. 5 shows the comparison of the two different CXTFIT simulations for the

Table 5
Transport parameters estimated by CXTFIT from Br^- and EC-derived LiCl BTCs obtained for Column 1 and Column 2.

	Column 1				Column 2			
	Br^- ADE	Br^- DD	LiCl ADE	LiCl DD	Br^- ADE	Br^- DD	LiCl ADE	LiCl DD
	IC	IC	EC	EC	IC	IC	EC	EC
λ_L (mm)	8.89	5.85	21.08	11.64	8.84	1.36	14.48	5.55
α (1/d)	n.a.	0.297	n.a.	0.265	n.a.	0.832	n.a.	0.177
θ_m (−)	0.392	0.356	0.392	0.348	0.416	0.226	0.416	0.331
θ_{im} (−)	n.a.	0.039	n.a.	0.044	n.a.	0.190	n.a.	0.085
R^2	0.920	0.996	0.965	0.988	0.852	0.982	0.889	0.993

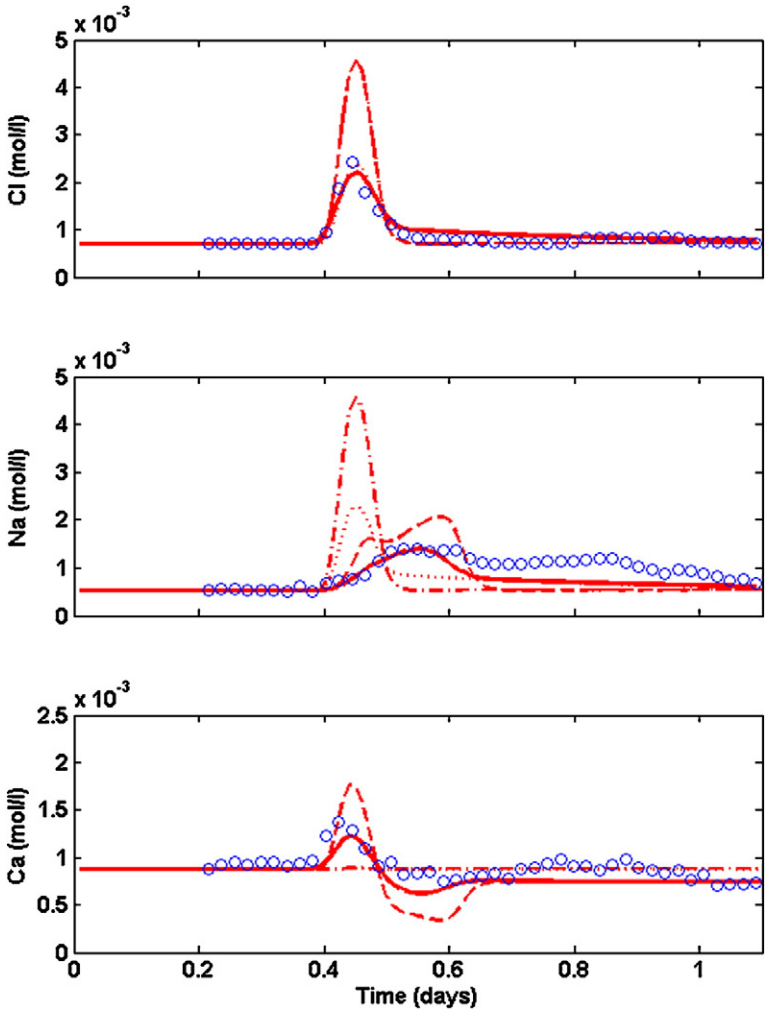

Fig. 4. Comparison of measured Cl^-, Na^+ and Ca^{2+} breakthrough curves (dots) versus results obtained with PHT3D for various, alternative process models: ADE without cation exchange (dashed dotted lines), DD without cation exchange (dotted lines), ADE with cation exchange (dashed lines) and DD with cation exchange (solid lines).

same experiment (both using the DD approach), one in which the EC-derived BTC for the NaCl tracer experiment was fitted and a second simulation in which the IC-determined Cl^- BTC was fitted. The EC-derived BTC for NaCl led to a different set of parameter values, which, as discussed before, can be attributed to the exchange reactions between Na^+, Ca^{2+} and Mg^{2+}, which are not accounted for in CXTFIT. The reactive transport model simulation for this specific experiment quantified simultaneously the mass-transfer processes and retardation induced by immobile zones and heterovalent cation exchange reactions. Note, that if the same model parameters (θ_m, θ_{im}, α and λ_L) are used, CXTFIT and the reactive transport model simulations agree for conservative species, as expected (Table 6). This is shown in Fig. 5, where only minor differences between the simulated Cl^- BTCs persist.

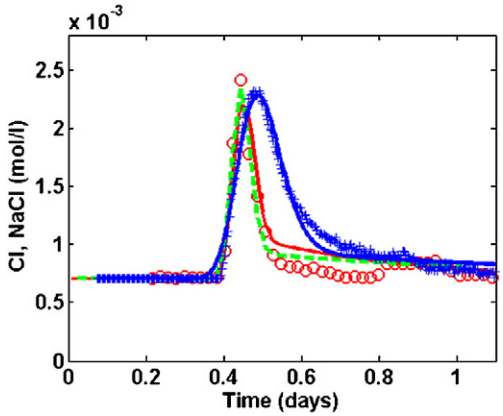

Fig. 5. Comparison of measured Cl^- (circles) versus PHT3D with DD (red line) and versus CXTFIT with DD (dashed green line); the NaCl derived BTC (crosses) versus CXTFIT with DD (blue line) is also plotted.

4. Conclusions and implications for field tracer tests

Usually electrolytic tracers are employed for subsurface characterisation, but the interpretation of tracer test data

Table 6
Model parameters used in the reactive transport and nonreactive simulations with DD approach of the NaCl tracer experiment in Column 2.

Parameter	PHT3D (Cl^-)	CXTFIT (Cl^-)	CXTFIT (EC)
θ_{im} (−)	0.23	0.198	0.23
α (1/d)	0.90	0.87	0.31
CEC[a] (meq/L)	2.40	–	–
λ_L (mm)	0.90	1.22	10.12

[a] The same CEC was used for mobile and immobile domain.

collected by low-cost techniques such as EC logging can be biased by cation exchange reactions. Therefore, it can be beneficial to assess the aquifer's CEC and its potential effect on the selected electrolytic tracer prior to field tracer experiments, as even sediments with medium to low CEC can induce deviations from the generally assumed linear relationship between EC and dissolved salt concentration. Reactive transport modelling allowed for a comprehensive and plausible quantification of observed data by considering both physical non-equilibrium transport processes and cation exchange reactions. The test procedure shown here can provide some guidance on the selection of the best electrolytic tracer that most closely mimics conservative species behaviour.

Acknowledgments

We are grateful Umberto Tessari and Enzo Salemi for the sediment characterisation and for the various discussions on sediment reactivity. We also thank Greg B. Davis and Janek Greskowiak for the constructive suggestions. The work presented in this paper was made possible and financially supported by EVIREN project, under PRITT fund (project FE-120).

References

Accinelli, C., Vicari, A., Rossi Pisa, P., Catizone, P., 2002. Losses of atrazine, metolachlor, prosulfuron and triasulfuron in subsurface drain water, I. Field results. Agronomie 22, 399–411.
Appelo, C.A.J., Postma, D., 2005. Geochemistry, groundwater and pollution, 2nd Edition. Balkema, Rotterdam, The Netherlands.
Atekwana, E.A., Atekwana, E.A., Rowe, R.S., Werkema Jr., D.D., Legall, F.D., 2004. The relationship of total dissolved solids measurements to bulk electrical conductivity in an aquifer contaminated with hydrocarbon. J. Appl. Geophys. 56 (4), 281–294.
Barra Caracciolo, A., Giuliano, G., Grenni, P., Guzzella, L., Pozzoni, F., Bottoni, P., Fava, L., Crobe, A., Orru`, M., Funari, E., 2005. Degradation and leaching of the herbicides metolachlor and diuron: a case study in an area of Northern Italy. Environ. Pollut. 134, 525–534.
Benker, E., Davis, G.B., Barry, D.A., 1997. Factors controlling the distribution and transport of trichloroethene in a sandy aquifer — hydrogeology and results of an in situ transport experiment. J. Hydrol. 202 (1–4), 315–340.
Brambati, A., Candian, C., Bisiacchi, G., 1973. Fortran IV program for settling tube size analysis using CDC 6200 computer. Istituto di Geologia e Paleontologia, Università di Trieste.
Burbery, L., Cassiani, G., Andreotti, G., Ricchiuto, T., Semple, K.T., 2004. Single-well reactive tracer test and stable isotope analysis for determination of microbial activity in a fast hydrocarbon-contaminated aquifer. Environ. Pollut. 129, 321–330.
Cassiani, G., Bruno, V., Villa, A., Fusi, N., Binley, A.M., 2006. A saline trace test monitored via time-lapse surface electrical resistivity tomography. J. Appl. Geophys. 59, 244–259.
Chen, J.S., Chen, Ch.S., Gau, H.S., Liu, Ch.W., 1999. A two well method to evaluate transverse dispersivity for tracer tests in a radially convergent flow field. J. Hydrol. 223, 175–197.
Choi, N.C., Kim, D.J., Kim, S.B., 2007. Quantification of bacterial mass recovery as a function of pore-water velocity and ionic strength. Res. Microbiol. 158, 70–78.
Cirpka, O.A., Fienen, M.N., Hofer, M., Hoehn, E., Tessarini, A., Kipfer, R., Kitanidis, P.K., 2007. Analyzing bank filtration by deconvoluting time series of electric conductivity. Ground Water 45 (3), 318–328.
Colombani, N., Mastrocicco, M., Gargini, A., Davis, G.B., Prommer, H., 2009. Modelling the fate of styrene in a mixed petroleum hydrocarbon plume. J. Contam. Hydrol. 105 (1–2), 38–55.
Comegna, V., Coppola, A., Sommella, A., 1999. Nonreactive solute transport in variously structured soil materials as determined by laboratory-based time domain reflectometry (TDR). Geoderma 92, 167–184.
Davis, S.N., Campbell, D.J., Bentley, H.W., Flynn, T.J., 1985. Groundwater tracers. National Ground Water Association, Dublin, Ohio.
Eriksson, N., Gupta, A., Destouni, G., 1997. Comparative analysis of laboratory and field tracer tests for investigating preferential flow and transport in mining waste rock. J. Hydrol. 194, 143–163.
Giddings, J.C., 1965. In dynamics of chromatography. M. Dekker, New York.
Giuliano, G., 1995. Ground water in the PO basin: some problems relating to its use and protection. Sci. Total Environ. 171, 17–27.
Greskowiak, J., Prommer, H., Liu, C., Post, V. E. A., Ma, R., Zheng, C., and Zachara, J., 2010. Impact of field-scale characteristics on parameter sensitivities in a dual-porosity, distributed-rate reactive system of uranium transport. Water. Resour. Res. 46, W09509. doi:10.1029/2009WR008781.
Guber, A.K., Shelton, D.R., Pachepsky, Ya.A., 2005. Transport and retention of manure-borne coliforms in soil. Vadose Zone J. 4, 828–837.
Hördt, A., Blaschek, R., Kemna, A., Zisser, N., 2007. Hydraulic conductivity estimation from induced polarization data at the field scale — the Krauthausen case history. J. Appl. Geophys. 62, 33–46.
Käss, W., 1998. Tracing technique in geohydrology. Balkema, Rotterdam.
King, R.S., Julstrom, B., 1982. Applied statistics using the computer. Alfred Publishing Company, Sherman Oaks, California.
Lyman, W.J., Reehl, W.F., Rosenblatt, D.H., 1990. Handbook of chemical property estimation methods. Am. Chem. Soc., Washington.
Mastrocicco, M., Colombani, N., Palpacelli, S., 2009. Fertilizers mobilization in alluvial aquifer: laboratory experiments. Environ. Geol. 56, 1371–1381.
Munoz-Carpena, R., Regalado, C.M., Ritter, A., Alvarez-Benedí, J., Socorro, A.R., 2005. TDR estimation of electrical conductivity and saline solute concentration in a volcanic soil. Geoderma 124, 399–413.
Onorati, G., Di Meo, T., Bussettini, M., Fabiani, C., Farrace, M.G., Fava, A., Ferronato, A., Mion, F., Marchetti, G., Martinelli, A., Mazzoni, M., 2006. Groundwater quality monitoring in Italy for the implementation of the EU water framework directive. Physics and Chemistry of the Earth, Parts A/B/C 31–17, 1004–1101.
Prommer, H., Barry, D.A., Zheng, C., 2003. PHT3D — A MODFLOW/MT3DMS based reactive multi-component transport model. Ground Water 42 (2), 247–257.
Ptak, T., Piepenbrink, M., Martac, E., 2004. Tracer tests for the investigation of heterogeneous porous media and stochastic modelling of flow and transport — a review of some recent developments. J. Hydrol. 294, 122–163.
Rajaram, H., Gelhar, L.W., 1991. Three-dimensional spatial moments analysis of the Borden tracer test. Water Resour. Res. 27 (6), 1239–1251.
Rein, A., Hoffmann, R., Dietrich, P., 2004. Influence of natural time-dependent variations of electrical conductivity on DC resistivity measurements. J. Hydrol. 285 (1–4), 215–232.
Rhoades, J.D., Manteghi, N.A., Shouse, P.J., Alves, W.J., 1989. Soil electrical conductivity and soil salinity: new formulations and calibrations. Soil Sci. Soc. Am. J. 52, 433–439.
Slater, L., 2007. Near surface electrical characterization of hydraulic conductivity: from petrophysical properties to aquifer geometries — a review. Surv. Geophys. 28 (2–3), 169–197.
Sudicky, E.A., 1986. A natural gradient experiment on solute transport in a sand aquifer: spatial variability of hydraulic conductivity and its role in the dispersion process. Water Resour. Res. 22, 2069–2082.
Sullivan, E.J., Reimus, P.W., Couce, D.A., 2003. Transport of a reactive tracer in saturated alluvium described using a three component cation exchange model. J. Contam. Hydrol. 62–63, 675–694.
Sutton, D.J., Kabala, Z.J., Schaad, D.E., Ruud, N.C., 2000. The dipole-flow test with a tracer: a new single-borehole tracer test for aquifer characterization. J. Contam. Hydrol. 44, 71–101.
Thierrin, J., Davis, G.B., Barber, C., 1995. A groundwater tracer test with deuterated compounds for monitoring in situ biodegradation and retardation of aromatic compounds. Ground Water 33 (3), 469–475.
Toride, N., Leji, F.J., van Genuchten, M.Th., 1999. The CXTFIT code for estimating transport parameters from laboratory or field tracer experiments. : Version

2.1. Research Report, vol. 137. U.S. Salinity Laboratory, Agricultural Research Service, U.S. Dept. of Agriculture, Riverside, CA.
Valocchi, A.J., 1985. Validity of the local equilibrium assumption for modeling sorbing solute transport through homogeneous soils. Water Resour. Res. 21, 808–820.
van Genuchten, M.Th., Wierenga, P.J., 1976. Mass transfer studies in sorbing porous media, I. Analytical solutions. Soil Sci. Soc. Am. J. 40 (4), 473–480.
Vincent, A., Benoit, P., Pot, V., Madrigal, I., Delgado-Moreno, L., Labat, C., 2007. Impact of different and uses on the migration of two herbicides in a silt loam soil: unsaturated soil column displacement studies. Eur. J. Soil Sci. 58, 320–328.
Vogt, T., Hoehn, E., Schneider, P., Freund, A., Schirmer, M., Cirpka, O.A., 2010. Fluctuations of Electrical Conductivity as a Natural Tracer for Bank Filtration in a Losing Stream. Adv. Water Res. 33 (11), 1296–1308.